Quantum coherence enhanced carrier lifetime of WS_2 nanotubes: A time-domain *ab initio* study

Tingbo Zhang,[1,*] Zhaobo Zhou,[1,*] Yehui Zhang,[1] Xianghong Niu,[2] Ming-Gang Ju,[1] Qian Chen,[1,†] and Jinlan Wang[1,3,‡]

[1]*School of Physics, Southeast University, Nanjing 211189, China*

[2]*New Energy Technology Engineering Laboratory of Jiangsu Province, School of Science, Nanjing University of Posts and Telecommunications (NJUPT), Nanjing 210023, China*

[3]*Synergetic Innovation Center for Quantum Effects and Applications (SICQEA), Hunan Normal University, Changsha 410081, China*

(Received 13 January 2022; revised 23 August 2022; accepted 9 November 2022; published 28 November 2022)

Transition-metal dichalcogenide (TMD) nanotubes with small band gap exhibit higher photocurrent than their layered counterparts [J. H. Smet and Y. Iwasa, Nature (London) **570**, 349 (2019); X. Zhou *et al.*, Small **15**, 1902528 (2019)], but the mechanism remains unclear. Herein, using WS_2 as an example, we revealed that the higher photovoltaic effect of the nanotubes originates from the quantum coherence between the band edges in the perspective of photogenerated carrier recombination. By using first-principles calculations and nonadiabatic molecular dynamics simulations, we revealed that small nonadiabatic coupling and short pure-dephasing time improve the photogenerated carrier lifetime and increase the photocurrent of WS_2 nanotubes. Moreover, an extremum of carrier lifetime in WS_2 nanotubes is found at a certain diameter, where the nanotube exhibits the longest carrier lifetime. The insights into the high photocurrent of TMD nanotubes may provide ideas for the design of advanced optoelectronic devices.

DOI: 10.1103/PhysRevB.106.205308

I. INTRODUCTION

Transition-metal dichalcogenides (TMDs) have become one of the star materials due to their high surface area, strong light-matter interaction, and high photoelectric response [1–3]. Most TMD monolayers (MLs) are semiconductors with band gap of 1.2 ∼ 2.1 eV, which can effectively utilize visible and near-infrared light [4–7]. Therefore, TMD MLs have been widely studied in photovoltaics, photodetection, and photocatalysis [7–9] For example, Lopez-Sanchez *et al.* found that phototransistors based on MoS_2 ML exhibit high photoresponsivity, about 10^6 times as high as graphene-based phototransistors [8]. However, the lifetime of the photogenerated electron-hole (e-h) pairs in TMD MLs is very short, on the order of picosecond (ps). Rapid carrier recombination often has an adverse effect on the light-to-current conversion [10–13]. One way to improve the photogenerated carrier lifetime of 2D materials is to roll MLs into nanotubes (NTs) [14–23]. The photogenerated carrier lifetime of carbon NTs is found 54 times longer than that of graphene nanoribbons, which is attributed to the weaker electron-phonon (e-ph) scattering in the carbon NTs [17]. Zhou *et al.* also found that the photoresponsivity and photosensitivity of $MoSe_2$ NTs are dozens of times larger than those of $MoSe_2$ layers [23]. Zhang *et al.* unveiled that the photovoltaic effect of WS_2 NTs is two orders of magnitude higher than that of WS_2 ML [4]. However, both experimental and theoretical results demonstrated that the band gaps of TMD NTs are smaller than those of TMD MLs [24,25]. According to the energy-gap law [26], a smaller band gap usually facilitates the photogenerated carrier recombination. Therefore, the reason why the TMD NTs have higher photocurrent than their layered counterparts remains unclear.

In this work, we studied the electronic structure and carrier lifetime of WS_2 ML and NTs by employing first-principles calculations and nonadiabatic molecular dynamics (NAMD) simulations. We found that the rapid pure-dephasing time stemming from the structural effect prolongs the carrier lifetime, which should greatly increase the photocurrent of WS_2 NTs. NAMD calculations show that the e-h recombination time of (22, 0) NTs is 5.22 ns, about 11 times longer than WS_2 ML. It is revealed that the two combinative factors of nonadiabatic coupling (NAC) and pure-dephasing time dominate the carrier lifetime of WS_2 NTs, which provides theoretical guidance for the experimental preparation of high-performance photoelectric devices.

II. COMPUTATIONAL METHODS

The structural optimization and electronic structure of WS_2 ML and NTs were calculated by using the Vienna *Ab initio* Simulation Package based on density-functional theory [27]. The generalized gradient approximation exchange-correlation functional was adopted in form of the Perdew-Burke-Ernzerhof method [28,29]. An energy cutoff of 500 eV was set for the electronic wave-function expansion. All structures were fully relaxed until the force on each atom converged to smaller than 0.02 eV/Å. The vacuum layers of more than 15 Å were applied to avoid interaction between adjacent periods and the $7 \times 7 \times 1$ and $1 \times 1 \times 11$ k points were used for the calculations of WS_2 ML and NTs, respectively.

To simulate the e-h recombination process, NAMD calculations based on the PYXAID code were performed by using

*These authors contributed equally to this work.
†Corresponding author: qc119@seu.edu.cn
‡Corresponding author: jlwang@seu.edu.cn

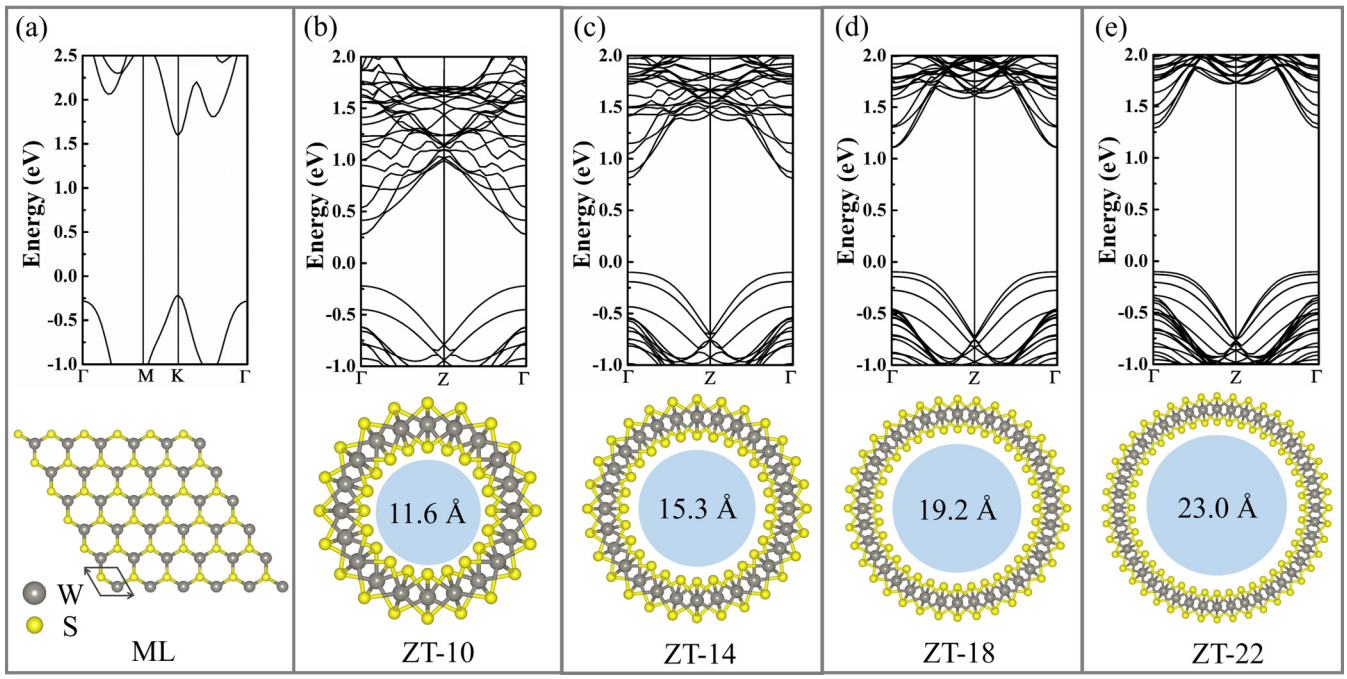

FIG. 1. Band structure and optimized atomic structure of WS_2: (a) ML, (b) ZT-10, (c) ZT-14, (d) ZT-18, and (e) ZT-22.

the decoherence-induced surface-hopping method [30–32]. At first, the 6 × 6 WS_2 ML and NTs with different diameters were relaxed at 0 K. Afterwards, a 5-ps heating process from 0 to 300 K was made. As shown in the Supplemental Material [33], large structural deformation was not observed during the heating process for WS_2. Next, the adiabatic molecular dynamics (MD) trajectories of 4 ps were generated with the microcanonical ensemble in a time interval of 1 fs. The Hamiltonian of nonadiabatic coupling was obtained by calculating the electronic structure of each MD trajectory. The e-h recombination process was simulated by averaging 200 initial configurations in the first 1-ps MD. Starting from each initial configuration, NAMD simulations were carried out by using 3000 random number sequences for surface-hopping probability.

III. RESULTS AND DISCUSSION

A. Electronic structure

Previous work reported that the WS_2 NTs prepared in the experiment are polar and with noncentrosymmetric symmetry [4]; therefore, we focused on the zigzag WS_2 NTs in this work as the armchair NTs are nonpolar and centrosymmetric. Four zigzag NTs with different diameters were considered: (10, 0), (14, 0), (18, 0), and (22, 0), named as ZT-10, ZT-14, ZT-18, and ZT-22, respectively. Their band structures are depicted in Fig. 1 together with that of WS_2 ML for comparison. The band gap of WS_2 NTs monotonically increases from 0.50 to 1.39 eV as the diameter of the tubes increases (listed in Table I), consistent with the previously reported results [34–36].

The W–S bonds inside and outside the WS_2 NTs have different bond length (see Supplemental Material [33]) and result in the redistribution of the charge density. To illustrate the variation of the internal charge distribution, a quantitative electron transfer between the W and S atoms on different sides was calculated by the Bader charge analysis [37]. As shown in Fig. 2(a), the electrons obtained by the outer S atoms are more than the inners. This redistribution is also reflected in the electrostatic potential of WS_2 NTs. As depicted in Fig. 2(b) and Fig. S2 (see Supplemental Material [33]), different from WS_2 ML, the asymmetric electrostatic potential between two S layers in WS_2 NTs forms a dipole pointing in the radial direction. This potential difference can suppress the e-h recombination [38], which prolongs the photogenerated carrier lifetime and enhances the photocurrent. The spatial structure of wave functions at conduction-band minimum (CBM) and valence-band maximum (VBM) was further explored and displayed in Fig. 2(d). For WS_2 ML, the state density at both CBM and VBM are all around the W atoms and dominates by the W-*d* orbitals. The full overlapping of CBM and VBM in the real space is detrimental to the e-h separation, while for WS_2 NTs, the state density at the VBM spread on the W and the outer S atoms. More precisely, the CBM of NTs is still dominated by the W-*d* orbitals, while the VBM is contributed by both W-*d* and S-*p* orbitals, as shown in Fig 2(c). The spatial separation of the states at CBM and VBM can help to separate the e-h pair, which is crucial for a long

TABLE I. The band gap, NAC, pure-dephasing time, and photon-generated carrier lifetime of WS_2 ML, ZT-10, ZT-14, ZT-18, and ZT-22.

	Band gap (eV)	NAC (meV)	Pure dephasing (fs)	Lifetime (ns)
ML	1.81	0.77	33.0	0.48
ZT-10	0.50	2.42	7.8	0.04
ZT-14	0.91	0.81	7.5	0.30
ZT-18	1.20	0.31	5.4	2.55
ZT-22	1.39	0.28	7.0	5.22

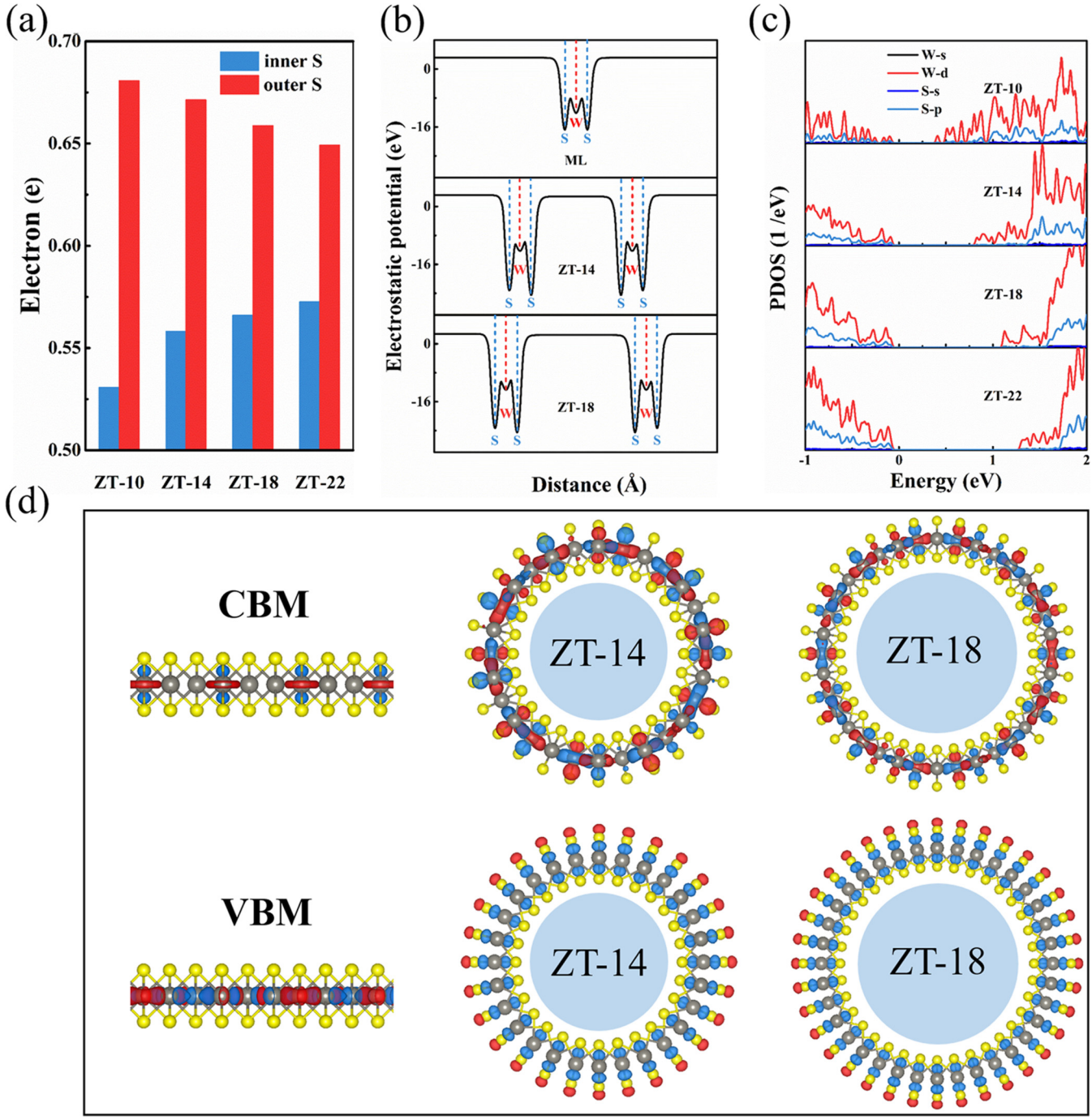

FIG. 2. (a) Bader charge of ZT-10, ZT-14, ZT-18 and ZT-22. (b) Electrostatic potential of WS_2 ML, ZT-14, and ZT-18. (c) Partial density of states (PDOS) of ZT-10, ZT-14, ZT-18, and ZT-22. (d) Spatial structure of wave functions at CBM (upper) and VBM (down) of WS_2 ML, ZT-14, and ZT-18. The red and blue represent the positive and negative wave functions, respectively.

carrier lifetime. However, such qualitative prediction of the carrier lifetime based on the electronic structure is inadequate as the electron-phonon (e-ph) coupling effect also plays an important role in determining e-h recombination. The carrier-dynamics behavior should be further explored.

B. Photogenerated carrier lifetime

To quantitatively assess the difference in carrier lifetime between WS_2 ML and NTs, the e-h recombination rate was calculated by using NAMD simulations. The electrons can be excited from the VB to the CB and form holes at VB after light absorption [progress ① in Fig. 3(a)]. Meanwhile, the photogenerated electrons at the CBM recombine with the holes at the VBM [progress ② in Fig. 3(a)] [39]. To determine the carrier lifetime (τ), we fitted the NAMD data with the formula of a short-time linear approximation to the exponential decay: $f(t) = \exp(-t/\tau)$, according to the previous literature [5,11,13]. The predicted carrier lifetime of WS_2 ML is 482 ps, consistent with the reported experimental results [2,40]. Note

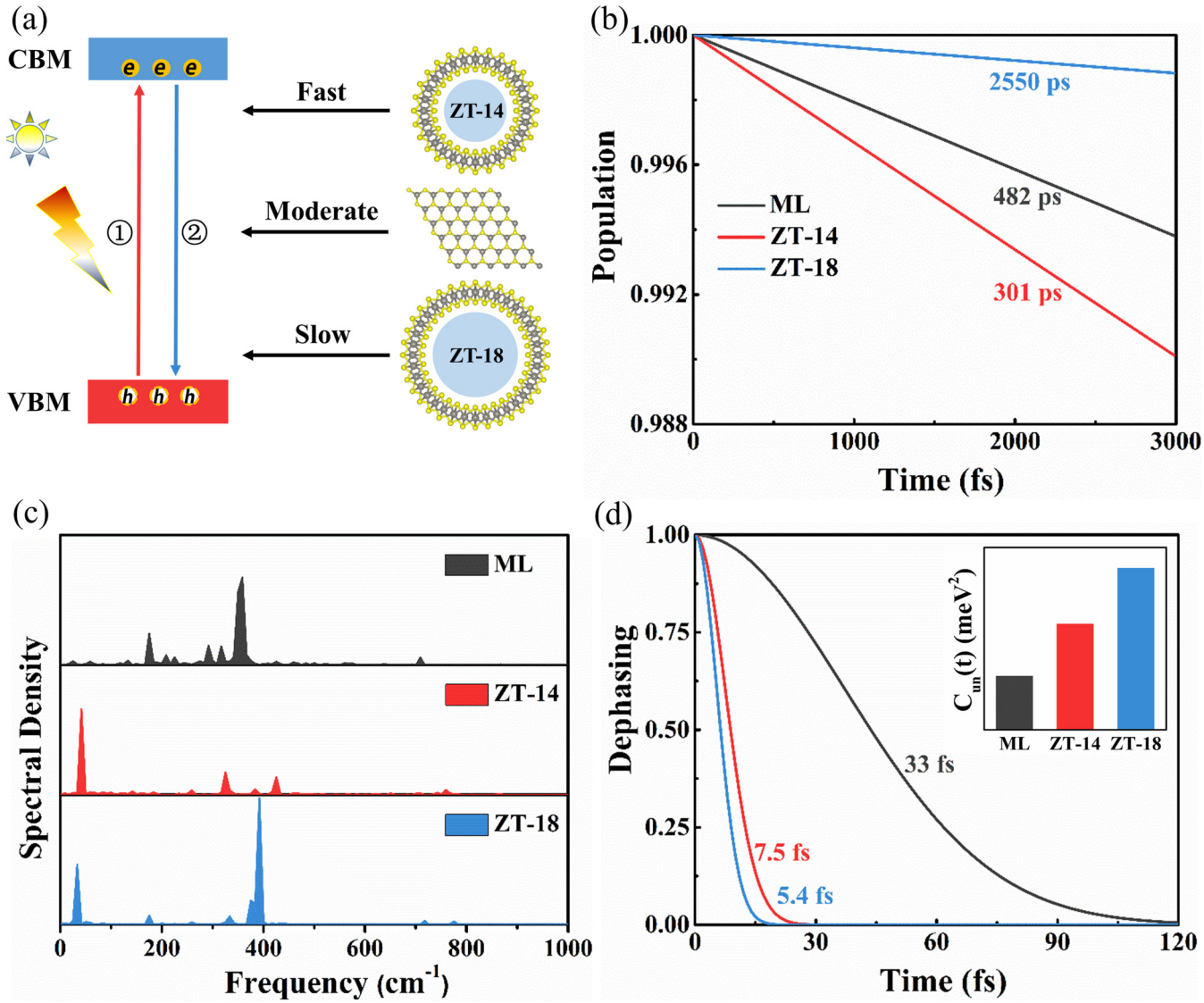

FIG. 3. (a) Diagram of e-h recombination of WS_2 ML and NTs. (b) The e-h recombination time, (c) FT spectra, and (d) pure-dephasing time of WS_2 ML, ZT-14, and ZT-18; the inset shows the un-ACFs. The amplitudes of ZT-14 and ZT-18 are reduced by 5 and 10 times in FT spectra, respectively.

that the carrier lifetime of WS_2 NTs increases along with their diameter, as listed in Table I. In particular, the carrier lifetime of WS_2 NTs with larger diameters (ZT-18 and ZT-22) is much longer than that of WS_2 ML. Such a long carrier lifetime corresponds with the discovered higher photocurrent of WS_2 NTs than ML in the experiment [4].

To reveal the underlying physics of the different carrier lifetimes of WS_2 NTs, the NAC between CBM and VBM was calculated as listed in Table I. The NAC matrix element d_{jk} can be expressed as

$$d_{jk} = \left\langle \varphi_j \left| \frac{\partial}{\partial t} \right| \varphi_k \right\rangle = \frac{\langle \varphi_j | \nabla_R H | \varphi_k \rangle}{\varepsilon_k - \varepsilon_j} \dot{R}, \tag{1}$$

where H is the Hamiltonian of Kohn-Sham; φ_j and φ_k represent the wave function of electronic states k and j, respectively. The ε_k and ε_j are the corresponding eigenvalues, and $\dot{R}$ represents the nuclear velocity. Here, the states k and j stand for the CBM and VBM. Small NAC weakens the coupling of the wave function and tends to suppress the e-h recombination [41], thus leading to a long carrier lifetime. According to formula (1), the NAC is inversely proportional to the term of energy difference $(\varepsilon_k - \varepsilon_j)$ and positively proportional to the terms of e-ph coupling $(\langle \varphi_j | \nabla_R H | \varphi_k \rangle)$ and the nuclear velocity $(\dot{R})$. This means all the WS_2 NTs with smaller band gaps are expected to have larger NAC than that of ML. However, the NAMD calculations revealed that only ZT-10 and ZT-14 have larger NAC values (2.42 and 0.81 meV). The smaller NAC of ZT-18 and ZT-22 indicates that more complicated e-ph scattering also plays an important role in the e-h recombination process of these NTs.

The Fourier transform (FT) spectrum regarding the energy shift of the initial and final state is depicted in Fig. 3(c). Compared with ML, the WS_2 NTs exhibit relatively low-frequency

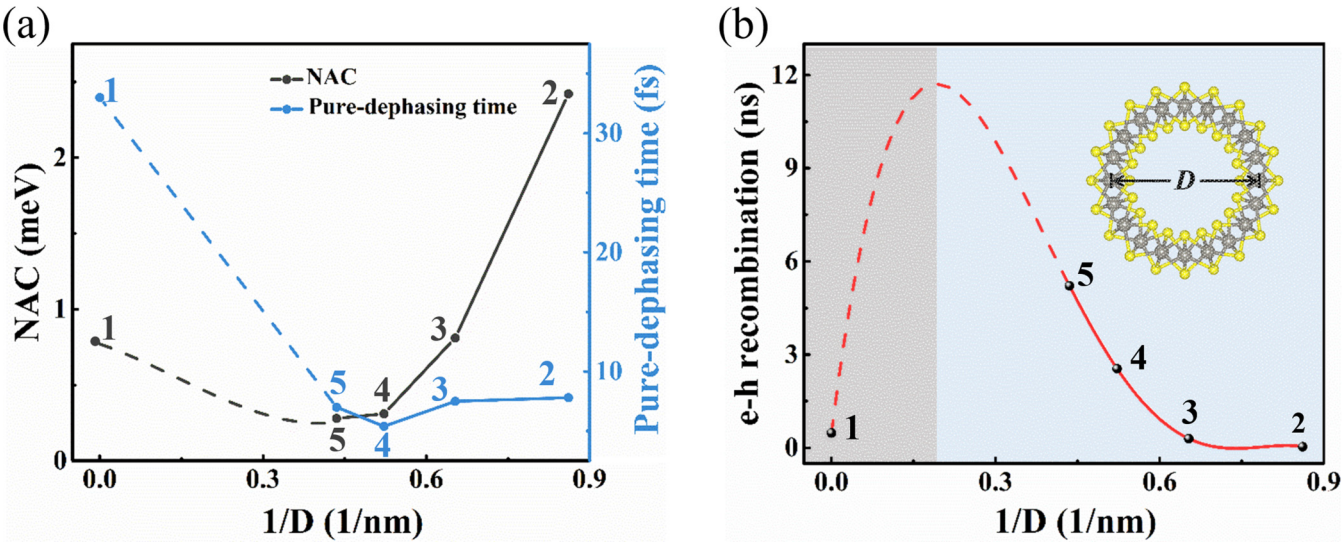

FIG. 4. (a) NAC and pure-dephasing time of WS_2 ML and NTs with different diameters. The solid and dotted lines are used to guide the eyes. (b) Predicted relationship between e-h recombination time and diameter of the WS_2 NTs. The dots of 1, 2, 3, 4, and 5 in (a) and (b) represent WS_2 ML, ZT-10, ZT-14, ZT-18, and ZT-22, respectively.

peaks, indicating that the phonon mode with lower frequency reduces the e-ph scattering. In addition, these low-frequency modes also correspond with the decreased velocity of the nucleus [13], which has also been verified by the mean velocity of W atoms obtained from the MD simulations (see Supplemental Material [33]). According to formula (1), the lower velocity decreases the NAC, therefore prolonging the carrier lifetime. Based on the above results, we conclude that the carrier lifetime is closely related to the diameter of NTs. For NTs with larger diameters, the low-frequency phonon gives rise to small e-ph scattering, leading to a very small NAC and long carrier lifetime, while for NTs with smaller diameters, their small band gap brings large NACs and therefore accelerates the e-h recombination.

The pure-dephasing time is also an important factor affecting the e-h recombination. Generally speaking, short pure-dephasing time slows down the e-h recombination [13]. The pure-dephasing time can be defined by the second-order cumulant approximation [42]:

$$D_{ij}(t) = \exp\left[-\frac{1}{\hbar^2}\int_0^t dt' \int_0^{t'} dt'' C_{ij}(t'')\right], \tag{2}$$

where $C_{ij}(t)$ is the unnormalized autocorrelation function (un-ACF) of the fluctuations of the energy gap (δE_{ij}) between electronic states i and j, which can be defined by

$$C_{ij}(t) = \langle \delta E_{ij}(t')\delta E_{ij}(t - t^{'})\rangle_{t'}. \tag{3}$$

As shown in Fig. 3(d) and Fig. S3 (see Supplemental Material [33]), WS_2 NTs possess smaller pure-dephasing time in comparison with WS_2 ML, which is beneficial to suppressing the e-h recombination. Meanwhile, un-ACF is shown in Fig. 3(d). The square root of the initial ACF ($t = 0$ fs) represents the fluctuation amplitude of the band gap. A larger initial value of un-ACFs usually corresponds to a shorter pure-dephasing time [43]. As seen in Fig. 3(d), ZT-14 and ZT-18 have larger initial un-ACF than WS_2 ML, which means that the wave-function phase difference between CBM and VBM of the NTs accumulates faster than that of ML, thus reducing the pure-dephasing time. Specifically, for ML, the full overlapping of the wave functions at CBM and VBM indicates a long coherence. When WS_2 ML is rolled into NTs, the states at the VBM are partially dispersed to outer S atoms [see Fig. 2(d)], therefore reducing the coherence between CBM and VBM. Note that the pure-dephasing time of the four NTs shows no relevance to their radials, and is all about one order of magnitude smaller than the ML. This means the factor of the pure-dephasing time has an overall promotion for the carrier lifetime of WS_2 NTs within the gauge scale considered in this work.

C. Discussion

So far, we have found that the NAC of WS_2 NTs decreases along with their diameter [see in Fig. 4(a)], which arises from the combined effect of the band gap, nuclear velocity, and e-ph scattering. Note that the band gap increases along with the diameter of NTs and gradually converges to about 1.9 eV. After 5 nm, the band gap shows a weak correlation with the further increased diameter [44], while the nuclear velocity bottoms out and begins to rise when the diameter is larger than 2 nm (Supplemental Material [33]). This results in the NAC of the ML being higher than ZT-18 and ZT-22. In addition, although the pure-dephasing times of the WS_2 NTs are all much smaller than that of ML, the continuous increase of diameter would make it gradually rise and finally reach 33 fs of the ML. Therefore, for WS_2 NTs, the cooperation between NAC and pure-dephasing time would inevitably lead to a maximum of the carrier lifetime when it varies with the diameter, as shown in Fig. 4(b). Note that as the diameter of the TMD NTs prepared in the experiment is generally greater than 5 nm and their e-h recombination time is longer than the ML phase, we predict the relationship as shown in Fig. 4(b).

This explains the higher photoelectric/photovoltaic effect of TMD NTs reported by experimental groups [4,23].

IV. CONCLUSIONS

In summary, based on first-principles and NAMD calculations, we have studied the carrier lifetime of the WS_2 ML and NTs with different diameters. It is found that the small NAC and short pure-dephasing time improve the photogenerated carrier lifetime and increase the photocurrent of WS_2 NTs. Specifically, the carrier lifetime of ZT-18 and ZT-22 are, respectively, 5 and 11 times higher than that of WS_2 ML. By analyzing the relationship between carrier lifetime and different diameters, we predicted that NT with a diameter of about 5 nm has the longest carrier lifetime. This work provides an interpretation of the measured higher photovoltaic effect of WS_2 NTs than the ML. This mechanism may also apply to other TMD nanotubes and provide ideas for the future design of optoelectronic devices.

ACKNOWLEDGMENTS

This work is supported by the Basic Research Program of Jiangsu Province (Grant No. BK20222007), National Natural Science Foundation of China (Grants No. 21973011, No. 22033002, and No. 21525311) and the Fundamental Research Funds for the Central Universities. The authors acknowledge the computational resources from the Big Data Center of Southeast University and the National Supercomputing Center of Tianjin.

[1] T. Akamatsu, T. Ideue, L. Zhou, Y. Dong, S. Kitamura, M. Yoshii, D. Yang, M. Onga, Y. Nakagawa, K. Watanabe, T. Taniguchi, J. Laurienzo, J. Huang, Z. Ye, T. Morimoto, H. Yuan, and Y. Iwasa, Science **372**, 68 (2021).
[2] L. Li, R. Long, T. Bertolini, and O. V. Prezhdo, Nano Lett. **17**, 7962 (2017).
[3] S. Jia, Z. Jin, J. Zhang, J. Yuan, W. Chen, W. Feng, P. Hu, P. M. Ajayan, and J. Lou, Small **16**, 2002263 (2020).
[4] Y. J. Zhang, T. Ideue, M. Onga, F. Qin, R. Suzuki, A. Zak, R. Tenne, J. H. Smet, and Y. Iwasa, Nature (London) **570**, 349 (2019).
[5] Y. Yang, W. H. Fang, A. Benderskii, R. Long, and O. V. Prezhdo, J. Phys. Chem. Lett. **10**, 7732 (2019).
[6] C. Jin, E. Y. Ma, O. Karni, E. C. Regan, F. Wang, and T. F. Heinz, Nat. Nanotechnol. **13**, 994 (2018).
[7] M. Buscema, J. O. Island, D. J. Groenendijk, S. I. Blanter, G. A. Steele, H. S. van der Zant, and A. Castellanos-Gomez, Chem. Soc. Rev. **44**, 3691 (2015).
[8] O. Lopez-Sanchez, D. Lembke, M. Kayci, A. Radenovic, and A. Kis, Nat. Nanotechnol. **8**, 497 (2013).
[9] A. M. Schankler, L. Gao, and A. M. Rappe, J. Phys. Chem. Lett. **12**, 1244 (2021).
[10] L. Li, R. Long, and O. V. Prezhdo, Nano Lett. **18**, 4008 (2018).
[11] R. Long and O. V. Prezhdo, Nano Lett. **16**, 1996 (2016).
[12] X. Niu, G. Wu, X. Zhang, and J. Wang, Nanoscale **12**, 6057 (2020).
[13] Z. Zhou, Y. Zhang, X. Zhang, X. Niu, G. Wu, and J. Wang, J. Mater. Chem. A **8**, 20621 (2020).
[14] S. A. Jensen, R. Ulbricht, A. Narita, X. Feng, K. Mullen, T. Hertel, D. Turchinovich, and M. Bonn, Nano Lett. **13**, 5925 (2013).
[15] M. G. Burdanova, R. J. Kashtiban, Y. Zheng, R. Xiang, S. Chiashi, J. M. Woolley, M. Staniforth, E. Sakamoto-Rablah, X. Xie, M. Broome, J. Sloan, A. Anisimov, E. I. Kauppinen, S. Maruyama, and J. Lloyd-Hughes, Nano Lett. **20**, 3560 (2020).
[16] A. Albu-Yaron, S. S. Sinha, and R. Tenne, ACS Energy Lett. **5**, 1498 (2020).
[17] G. Zhou, C. Cen, S. Wang, M. Deng, and O. V. Prezhdo, J. Phys. Chem. Lett. **10**, 7179 (2019).
[18] P. Chithaiah, S. Ghosh, A. Idelevich, L. Rovinsky, T. Livneh, and A. Zak, ACS Nano **14**, 3004 (2020).
[19] A. Grillo, M. Passacantando, A. Zak, A. Pelella, and A. Di Bartolomeo, Small **16**, 2002880 (2020).
[20] F. Qin, T. Ideue, W. Shi, X. X. Zhang, M. Yoshida, A. Zak, R. Tenne, T. Kikitsu, D. Inoue, D. Hashizume, and Y. Iwasa, Nano Lett. **18**, 6789 (2018).
[21] F. Qin, W. Shi, T. Ideue, M. Yoshida, A. Zak, R. Tenne, T. Kikitsu, D. Inoue, D. Hashizume, and Y. Iwasa, Nat. Commun. **8**, 14465 (2017).
[22] R. Xiang, T. Inoue, Y. Zheng, A. Kumamoto, Y. Qian, Y. Sato, M. Liu, D. Tang, D. Gokhale, J. Guo, K. Hisama, S. Yotsumoto, T. Ogamoto, H. Arai, Y. Kobayashi, H. Zhang, B. Hou, A. Anisimov, M. Maruyama, Y. Miyata, S. Okada, S. Chiashi, Y. Li, J. Kong, E. I. Kauppinen, Y. Ikuhara, K. Suenaga, and S. Maruyama, Science **367**, 537 (2020).
[23] X. Zhou, Z. Tian, H. J. Kim, Y. Wang, B. Xu, R. Pan, Y. J. Chang, Z. Di, P. Zhou, and Y. Mei, Small **15**, 1902528 (2019).
[24] S. S. Sinha, A. Zak, R. Rosentsveig, I. Pinkas, R. Tenne, and L. Yadgarov, Small **16**, 1904390 (2020).
[25] G. Seifert, H. Terrones, M. Terrones, G. Jungnickel, and T. Frauenheim, Phys. Rev. Lett. **85**, 146 (2000).
[26] R. Englman and J. Jortner, J. Lumin **1**, 134 (1970).
[27] S. S. Sinha, L. Yadgarov, S. B. Aliev, Y. Feldman, I. Pinkas, P. Chithaiah, S. Ghosh, A. Idelevich, A. Zak, and R. Tenne, J. Phys. Chem. C **125**, 6324 (2021).
[28] J. Hafner, J. Comput. Chem. **29**, 2044 (2008).
[29] J. P. Perdew, K. Burke, and M. Ernzerhof, Phys. Rev. Lett. **77**, 3865 (1996).
[30] A. V. Akimov and O. V. Prezhdo, J. Chem. Theory Comput. **9**, 4959 (2013).
[31] A. V. Akimov and O. V. Prezhdo, J. Chem. Theory Comput. **10**, 789 (2014).
[32] H. M. Jaeger, S. Fischer, and O. V. Prezhdo, J. Chem. Phys. **137**, 22A545 (2012).
[33] See Supplemental Material at http://link.aps.org/supplemental/10.1103/PhysRevB.106.205308 for AIMD simulation of the WS_2 nanotubes, the electronic structure, and NAMD data of ZT-10 and ZT-22.
[34] H. H. Wu, Q. Meng, H. Huang, C. T. Liu, and X. L. Wang, Phys. Chem. Chem. Phys. **20**, 3608 (2018).
[35] X. Wu, Z. Xu, and X. Zeng, Nano Lett. **7**, 2987 (2007).

[36] A. E. G. Mikkelsen, F. T. Bölle, K. S. Thygesen, T. Vegge, and I. E. Castelli, Phys. Rev. Mater. **5**, 014002 (2021).
[37] J. Liu, J. Phys. Chem. C **119**, 28417 (2015).
[38] S. Zhang, H. Jin, C. Long, T. Wang, R. Peng, B. Huang, and Y. Dai, J. Mater. Chem. A **7**, 7885 (2019).
[39] L. Li and E. A. Carter, J. Am. Chem. Soc. **141**, 10451 (2019).
[40] P. Zereshki, P. Yao, D. He, Y. Wang, and H. Zhao, Phys. Rev. B **99**, 195438 (2019).
[41] H. Guo, W. Chu, Q. Zheng, and J. Zhao, J. Phys. Chem. Lett. **11**, 4662 (2020).
[42] Z. Zhang, W.-H. Fang, M. V. Tokina, R. Long, and O. V. Prezhdo, Nano Lett. **18**, 2459 (2018).
[43] W. Li, J. Liu, F.-Q. Bai, H.-X. Zhang, and O. V. Prezhdo, ACS Energy Lett. **2**, 1270 (2017).
[44] J. Dong, H. Hu, H. Li, and G. Ouyang, Phys. Chem. Chem. Phys. **23**, 20574 (2021).